

PAPER

[View Article Online](#)
[View Journal](#) | [View Issue](#)Cite this: *Catal. Sci. Technol.*, 2023, 13, 1459Regeneration of atomic Ag sites over commercial γ -aluminas by oxidative dispersion of Ag metal particles†Hiroe Kubota, Shinya Mine,  Takashi Toyao  and Ken-ichi Shimizu *

Ag(3 wt%)-loaded γ - Al_2O_3 ($\text{Ag}/\text{Al}_2\text{O}_3$) catalysts were prepared using four types of commercially available alumina powders (CTB, PUR, VGL, and CFF). Based on the support, the activity of these catalysts for the H_2 -assisted selective catalytic reduction (SCR) of NO by NH_3 or C_3H_6 decreased in the order $\text{CTB} > \text{PUR} > \text{VGL} > \text{CFF}$. After sintering treatment (H_2 reduction at 800 °C), the particle size of the Ag metal nanoparticles (NPs) changed and was found to be correlated with the catalytic activity ($\text{CTB} < \text{PUR} < \text{VGL} < \text{CFF}$). After re-oxidation of H_2 -reduced $\text{Ag}/\text{Al}_2\text{O}_3$ at 500 °C, the *in situ* infrared (IR) spectra showed negative bands at 3762 cm^{-1} due to the $\text{HO}-\mu_1\text{-Al}_{\text{VI}}$ site, where the band intensity increased in the order $\text{CTB} > \text{PUR} > \text{VGL} > \text{CFF}$. IR study of pyridine adsorbed on Ag-free γ - Al_2O_3 showed that the number of strong Lewis acid sites (unsaturated $\text{Al}_{\text{IV}}^{3+}$) increased in the same order, $\text{CTB} > \text{PUR} > \text{VGL} > \text{CFF}$, and the number of strong Lewis acid sites decreased when Ag was loaded on the supports. *In situ* X-ray absorption near-edge structure (XANES) and UV-vis studies of $\text{Ag}/\text{Al}_2\text{O}_3$ sintered under $\text{NO} + \text{O}_2$ at 400 °C showed oxidative redispersion of the Ag metal NPs to regenerate atomic Ag(I) sites. The amount of redispersed Ag metal and the initial rates of redispersion estimated from the *in situ* UV-vis results changed in the following order: $\text{CTB} > \text{PUR} > \text{VGL} > \text{CFF}$. These results suggest that the $\text{HO}-\mu_1\text{-Al}_{\text{VI}}$ site adjacent to the unsaturated $\text{Al}_{\text{IV}}^{3+}$ site on γ - Al_2O_3 is the anchoring site of the atomic Ag species, and the sintering resistance of $\text{Ag}/\text{Al}_2\text{O}_3$ increases with the number of $\text{HO}-\mu_1\text{-Al}_{\text{VI}}$ sites. During H_2 -assisted SCR, where both H_2 and $\text{NO} + \text{O}_2$ were co-fed to the catalysts, the number of highly dispersed Ag species (active sites) increased with the number of $\text{HO}-\mu_1\text{-Al}_{\text{VI}}$ sites; hence, NO conversion increased with the number of $\text{HO}-\mu_1\text{-Al}_{\text{VI}}$ sites on the support. The present results provide molecular-level insights into the design of sintering-resistant $\text{Ag}/\text{Al}_2\text{O}_3$ catalysts for SCR.

Received 14th November 2022,
Accepted 17th January 2023

DOI: 10.1039/d2cy01950g

rsc.li/catalysis

1. Introduction

γ -Alumina-supported silver ($\text{Ag}/\text{Al}_2\text{O}_3$) catalysts have long been studied as promising catalysts for the selective catalytic reduction (SCR) of NO_x by hydrocarbons (HC-SCR).^{1–5} HC-SCR by $\text{Ag}/\text{Al}_2\text{O}_3$ has been once commercialized for NO_x removal from diesel exhaust.⁵ It is well known that H_2 promotes the activity of $\text{Ag}/\text{Al}_2\text{O}_3$ for NH_3 -SCR and HC-SCR,^{6–13} and many studies have focused on H_2 -assisted SCR by NH_3 (H_2 - NH_3 -SCR)^{14–20} or by HC (H_2 -HC-SCR).^{6–13} After a long debate on the active Ag species in HC-SCR reactions,^{1,6,13,20} it was concluded that isolated Ag(I) sites are indispensable for achieving high-performance $\text{Ag}/\text{Al}_2\text{O}_3$ catalysts for SCR.¹³ Hence, $\text{Ag}/\text{Al}_2\text{O}_3$ for HC-SCR can be regarded as a rare example of a commercialized

single-atom catalyst (SAC). Small $\text{Ag}_n^{\delta+}$ clusters generated from the *in situ* reduction of Ag(I) species by H_2 or HCs during SCR promoted the reaction under certain conditions, whereas Ag metal nanoparticles (NPs) had an adverse effect on NO_x conversion as they promoted the non-selective oxidation of reductants.^{17,20} Our previous study on H_2 - NH_3 -SCR^{14–20} showed that isolated Ag(I) sites and small $\text{Ag}_n^{\delta+}$ clusters, which coexist under the reaction conditions, play important roles. Previous reports have suggested that compared to other transition metals, supported single-atom Ag and small Ag clusters are more susceptible to sintering at lower temperatures.^{21–24} In commercial SCR systems, $\text{Ag}/\text{Al}_2\text{O}_3$ catalysts are exposed to high-temperature conditions, which could result in catalyst deactivation due to sintering of the isolated Ag(I) species to Ag metal NPs. Redispersion of the aggregated Ag NPs is a potential strategy for the regeneration of sintered $\text{Ag}/\text{Al}_2\text{O}_3$ catalysts. We previously reported the oxidative dispersion of large Ag metal NPs to isolated Ag(I) cations on θ - Al_2O_3 .²⁵ However, the precise dispersion mechanism and the nature of the anchoring sites remain elusive.

Institute for Catalysis, Hokkaido University, N-21, W-10, Sapporo 001-0021, Japan.
E-mail: kshimizu@cat.hokudai.ac.jp

† Electronic supplementary information (ESI) available. See DOI: <https://doi.org/10.1039/d2cy01950g>



The structures of the metal anchoring sites on γ - Al_2O_3 were discussed.^{26,27} Among various sites, recent studies employing Al nuclear magnetic resonance (NMR) spectroscopy^{28–32} exclusively proposed the pentacoordinated $\text{Al}_{\text{V}}^{3+}$ site as anchoring sites of various metal clusters. However, Al NMR is not a sufficient tool for complete characterization of the anchoring sites as this technique is not suitable for identification of other sites such as surface octahedral ($\text{Al}_{\text{VI}}^{3+}$) and tetrahedral Al ($\text{Al}_{\text{IV}}^{3+}$) sites and Al–OH sites. In this regard, infrared (IR) spectroscopy using basic probe molecules^{33–39} is useful for characterizing surface Al sites with different coordination environments ($\text{Al}_{\text{VI}}^{3+}$, $\text{Al}_{\text{V}}^{3+}$, and $\text{Al}_{\text{IV}}^{3+}$) and different Al–OH groups.^{40,41} Based on NH_3 -IR study on $\text{Ag}/\gamma\text{-Al}_2\text{O}_3$ and $\gamma\text{-Al}_2\text{O}_3$, Zeng *et al.*¹³ proposed that the terminal hydroxyl (OH) groups on the (100) surface are the anchoring sites of the isolated $\text{Ag}(\text{i})$ cations, which act as catalytic sites for H_2 -assisted HC-SCR. We recently studied the reversible structural transformation between atomic $\text{Ag}(\text{i})$ and large Ag metal NPs on a $\text{Ag}/\text{Al}_2\text{O}_3$ catalyst using various *in situ* spectroscopic techniques, *ex situ* microscopy, and theoretical calculations.⁴² The on-top OH group on octahedral Al ($\text{HO}-\mu_1\text{-Al}_{\text{VI}}$) adjacent to the unsaturated $\text{Al}_{\text{IV}}^{3+}$ site anchors isolated Ag^+ in the form of $\text{AgO}-\mu_1\text{-Al}_{\text{VI}}$, which can be converted to Ag metal NPs and $\text{HO}-\mu_1\text{-Al}_{\text{VI}}$ during sintering under H_2 . Thereafter, under $\text{NO} + \text{O}_2$, the Ag metal NPs and $\text{HO}-\mu_1\text{-Al}_{\text{VI}}$ react to regenerate dispersed single-atom $\text{AgO}-\mu_1\text{-Al}_{\text{VI}}$. Because the SCR activity of $\text{Ag}/\text{Al}_2\text{O}_3$ depends strongly on the type of Al_2O_3 source,¹³ we hypothesized that the SCR activity of $\text{Ag}/\text{Al}_2\text{O}_3$ prepared with different alumina samples depends on the number of anchoring sites on the alumina samples.

Herein, we prepare $\text{Ag}/\text{Al}_2\text{O}_3$ catalysts with four types of commercial alumina and investigate the relationships between the relative number of $\text{HO}-\mu_1\text{-Al}_{\text{VI}}$ sites and (1) the number of unsaturated $\text{Al}_{\text{IV}}^{3+}$ sites, (2) the sintering resistance of $\text{Ag}/\text{Al}_2\text{O}_3$, (3) the rate of Ag redispersion, and (4) the catalytic activity of $\text{Ag}/\text{Al}_2\text{O}_3$. *In situ* X-ray absorption spectroscopy (XAS), ultraviolet-visible (UV-vis) spectroscopy, and infrared (IR) spectroscopy are employed to quantify these properties. We propose that our anchoring site model, the $\text{HO}-\mu_1\text{-Al}_{\text{VI}}$ site adjacent to the unsaturated $\text{Al}_{\text{IV}}^{3+}$ site, is a universal model for different alumina samples and that the SCR activity of $\text{Ag}/\text{Al}_2\text{O}_3$ increases with an increase in the number of anchoring sites.

2. Experimental methods

Preparation and characterization of catalysts

$\text{Ag}/\text{Al}_2\text{O}_3$ catalysts were prepared using an impregnation method, and four types of $\gamma\text{-AlOOH}$ (CTB, PUR, VGL, and CFF in Table 1) were impregnated with an aqueous solution of AgNO_3 , followed by evaporation to dryness at 60 °C, drying at 100 °C for 12 h, and calcination in air at 600 °C for 1 h. The impurities of CTB and PUR are less than 0.002%. The $\text{Ag}/\text{Al}_2\text{O}_3$ catalysts are designated as $\text{Ag}x/\text{Al}_2\text{O}_3$ or $\text{Ag}x/\text{CTB}$, where x denotes the Ag loading amount (wt%). $\gamma\text{-Al}_2\text{O}_3$ was prepared by calcination of $\gamma\text{-AlOOH}$ at 600 °C (1 h).

X-ray diffraction (XRD) patterns were obtained using a Rigaku MiniFlex II/AP diffractometer with $\text{Cu-K}\alpha$ radiation. Fig. S1† shows XRD patterns of the fresh $\text{Ag}(3 \text{ wt}\%)\text{-loaded Al}_2\text{O}_3$ after calcination at 600 °C. The result shows the absence of Ag metal NPs on $\text{Ag}(3)/\text{CTB}$ and $\text{Ag}(3)/\text{PUR}$. Transmission electron microscopy (TEM) data were acquired using a JEOL JEM-2200FS electron microscope.²⁷ ^{27}Al magic-angle spinning (MAS) NMR (^{27}Al NMR) measurements were performed on a Bruker DSX-300 spectrometer operating at 300 MHz with a 4 mm rotor. The Brunauer–Emmett–Teller (BET) surface areas of the $\gamma\text{-Al}_2\text{O}_3$ samples were determined by N_2 adsorption using an Autosorb 6AG instrument (Yuasa Ionics Co., Ltd., Japan).

In situ spectroscopy

In situ diffuse reflectance UV-vis spectra were recorded on a Jasco V-750 UV-vis spectrometer. The sintered $\text{Ag}3/\text{Al}_2\text{O}_3$ (15 mg) catalyst powder was placed in a diffuse reflectance cell with a quartz window connected to a gas flow system (100 mL min^{-1}). The light source was directed to the center of the integrating sphere through an optical fiber. BaSO_4 was used to collect background spectra. The reflectance was converted to the Kubelka–Munk function.

In situ diffuse reflectance infrared Fourier-transform (DRIFT) spectra of the OH stretching region of the powder sample (*ca.* 40 mg) were recorded on a Jasco FT/IR-4600 instrument (mercury cadmium telluride detector) equipped with an *in situ* flow cell with a CaF_2 window. *In situ* IR spectra of the adsorbed pyridine were recorded in transmission mode using a Jasco FT/IR-4600 spectrometer. A 40 mg self-supporting wafer sample (20 mm ϕ) was mounted on a flow-type quartz IR cell (CaF_2 windows) connected to a

Table 1 Properties of commercially available alumina and investigated catalysts

Sample	Product name	Manufacturer	S_{BET}^a	Phase ^b	NO conversion in $\text{H}_2\text{-NH}_3\text{-SCR}^c$ [%]	NO conversion in $\text{H}_2\text{-C}_3\text{H}_6\text{-SCR}^c$ [%]
CTB	Catapal® B	Sasol	218	γ	55	34
PUR	Puralox® SBa 200	Sasol	200	γ	38	30
VGL	Versal-Alumina VGL-15	UOP	166	γ	13	17
CFF	CFF-NP005-50	chemPUR	135	γ , (θ , α) ^d	13	14

^a BET surface area ($\text{m}^2 \text{g}^{-1}$) of $\gamma\text{-Al}_2\text{O}_3$ after calcination at 600 °C. ^b Crystal phase of alumina estimated by XRD. ^c NO conversion (%) by $\text{Ag}(3 \text{ wt}\%)\text{-loaded Al}_2\text{O}_3$ (40 mg) for $\text{H}_2\text{-NH}_3\text{-SCR}$ at 150 °C and $\text{H}_2\text{-C}_3\text{H}_6\text{-SCR}$ at 400 °C. ^d $\gamma\text{-Al}_2\text{O}_3$ was the main phase, but XRD lines corresponding to θ and $\alpha\text{-Al}_2\text{O}_3$ were observed as minor phases.



flow system (100 mL min^{-1}). Twenty spectra were collected at a resolution of 4 cm^{-1} and averaged to obtain a spectrum. The spectrum of the catalyst wafer, acquired at the measurement temperature under He, was subtracted from each spectrum.

Ag *K*-edge X-ray absorption spectra were recorded in transmission mode using the BL-14B2 beamline at the SPring-8 synchrotron radiation facility (Harima, Japan). A Si(311) single crystal was used to obtain monochromatic X-ray beams. A self-supporting wafer of the sample (approximately $7 \text{ mm } \phi$) was placed in an *in situ* quartz cell under a flow of a gas mixture diluted with He (500 mL min^{-1}) at atmospheric pressure. Normalization and linear combination fitting (LCF) analysis of the X-ray absorption near-edge structure (XANES) and curve-fitting analysis of the extended X-ray absorption fine structure (EXAFS) data were performed using the Athena software package.⁴³ For the LCF analysis, Ag^+ -exchanged Ag-CHA ($\text{Si/Al} = 11$) and 10 wt% Ag-loaded low-surface-area Al_2O_3 were used as reference compounds for the isolated Ag(I) and Ag metal NPs, respectively.⁴² Fourier transformation of the k^3 -weighted EXAFS data was carried out over the k range of $3\text{--}10 \text{ \AA}^{-1}$ and R range of $1.05\text{--}3.2 \text{ \AA}^{-1}$. Curve-fitting analysis was performed using Artemis, and the parameters for each shell were provided by FEFF6.

Catalytic reactions

$\text{H}_2\text{-NH}_3\text{-SCR}$ ($\text{H}_2 + \text{NO} + \text{NH}_3 + \text{O}_2$) and $\text{H}_2\text{-C}_3\text{H}_6\text{-SCR}$ ($\text{H}_2 + \text{NO} + \text{C}_3\text{H}_6 + \text{O}_2$) were performed using $\text{Ag}_3/\text{Al}_2\text{O}_3$ powder in a fixed-bed flow reactor (flow rate = 100 mL min^{-1}). The composition of the feed gas, $\text{H}_2/\text{NO}/(\text{NH}_3 \text{ or } \text{C}_3\text{H}_6)/\text{O}_2/\text{He}$, was 1%/500 ppm/500 ppm/10%/balance. The concentrations of the feed gas and products were measured using an online IR spectrometer (Jasco FT/IR-4600 with a TGS detector) equipped with a custom-built gas cell. The concentrations of NO, NO_2 , N_2O , C_3H_6 , and NH_3 were calculated based on calibration results. The reaction rates were estimated by changing the catalyst loading under conditions where the NO and NH_3 conversions were below 30%.

3. Results and discussion

SCR activity and structure of four $\text{Ag}_3/\text{Al}_2\text{O}_3$ catalysts

Four commercial alumina sources (CTB, PUR, VGL, and CFF) with different characteristics were used (Table 1). Ag_3 (3 wt%)-loaded on alumina (designated as Ag_3/CTB) was prepared by a conventional impregnation method.⁴² The NO conversion (Table 1) achieved with these catalysts in the H_2 -assisted SCR of NO by NH_3 and C_3H_6 was measured at 150 and 400°C , respectively, using a flow reactor. For both reactions, the NO conversion of Ag-loaded alumina depended on the type of

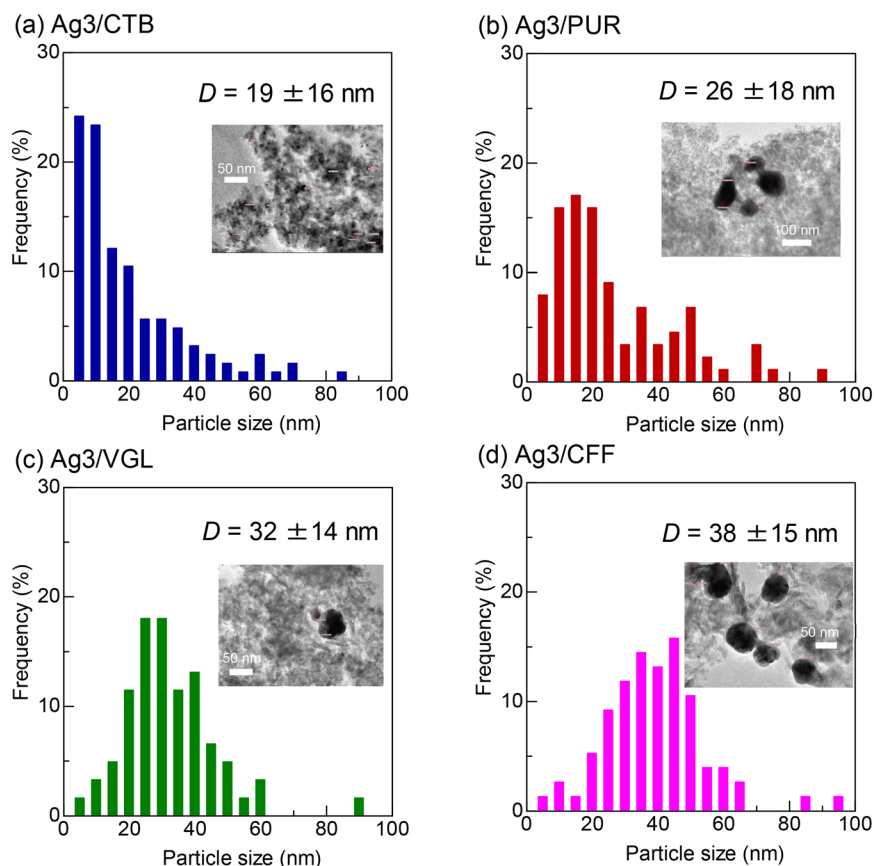


Fig. 1 Particle size distribution and TEM images of (a) Ag_3/CTB , (b) Ag_3/PUR , (c) Ag_3/VGL , and (d) Ag_3/CFF after sintering treatment (2% H_2 , 800°C , 0.5 h).



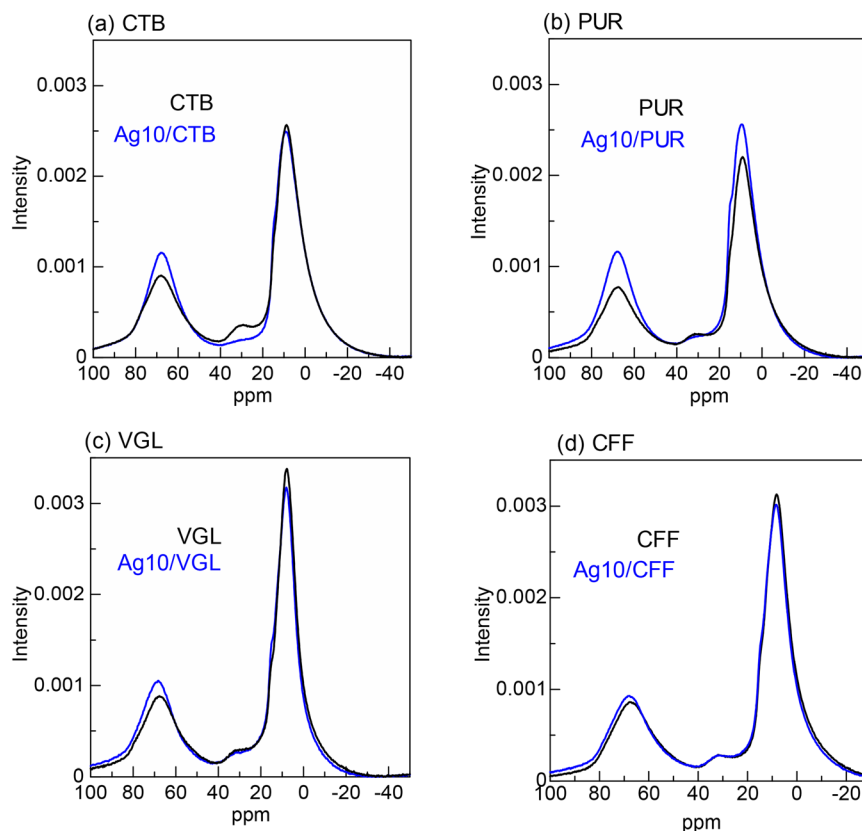


Fig. 2 ^{27}Al NMR spectra of $\gamma\text{-Al}_2\text{O}_3$ (black) and Ag(10 wt%)-loaded Al_2O_3 (blue): (a) CTB, (b) PUR, (c) VGL and (d) CFF. The samples were dehydrated under N_2 at 500 $^\circ\text{C}$ before the measurements.

alumina and increased in the order $\text{CTB} > \text{PUR} > \text{VGL} \geq \text{CFF}$.

The Ag-loaded alumina catalysts were reduced under a 2% H_2 flow at 800 $^\circ\text{C}$ (0.5 h) to prepare the sintered catalysts. The size distribution of the Ag NPs after sintering was estimated using *ex situ* TEM (Fig. 1). The mean diameter of the Ag metal NPs after the sintering treatment increased in the order $\text{CTB} < \text{PUR} < \text{VGL} < \text{CFF}$. The results indicate that the resistance to Ag sintering under reductive conditions depends on the type of alumina, and the sintering resistance decreased in the order $\text{CTB} > \text{PUR} > \text{VGL} > \text{CFF}$. This order is consistent with the order of the catalytic activity of Ag/ Al_2O_3 for SCR (Table 1).

Fig. 2 shows the ^{27}Al NMR spectra of the alumina and Ag-loaded alumina samples dehydrated at 500 $^\circ\text{C}$. To enhance the changes in the spectra caused by the loading of Ag, high-loading (10 wt%) samples were prepared and tested for ^{27}Al NMR measurements. The peaks with chemical shifts centered at 10, 33, and 67 ppm were assigned to $\text{Al}_{\text{IV}}^{3+}$, $\text{Al}_{\text{V}}^{3+}$, and $\text{Al}_{\text{VI}}^{3+}$, respectively. Previous ^{27}Al NMR studies of $\gamma\text{-Al}_2\text{O}_3$ have established that $\text{Al}_{\text{V}}^{3+}$ ions are present only on the first surface layer.²⁹ Upon loading 10 wt% Ag on CTB, the $\text{Al}_{\text{V}}^{3+}$ peak of CTB almost disappeared, indicating that some of the surface $\text{Al}_{\text{V}}^{3+}$ sites interacted with the Ag species. However, loading 10 wt% Ag on the other alumina samples (PUR, VGL, CFF) did not markedly change the intensity of the $\text{Al}_{\text{V}}^{3+}$

signals. These results demonstrate that ^{27}Al NMR is not a powerful method for investigating the anchoring sites of Ag species.

Our previous study⁴² showed that the IR spectra of Ag/ Al_2O_3 in the OH stretching region and pyridine adsorbed on Ag/ Al_2O_3 and Al_2O_3 are useful for discussing the anchoring site of isolated Ag^+ on Al_2O_3 . In brief, when Ag was loaded on Al_2O_3 , the IR peak at 3770 cm^{-1} assigned to the on-top OH group on octahedral Al ($\text{HO-}\mu_1\text{-Al}_{\text{VI}}$)³⁹ became less intense; the intensity of the band at 1621 cm^{-1} due to strong Lewis acid sites (unsaturated $\text{Al}_{\text{IV}}^{3+}$ sites) also declined. Combining the results of STEM and DFT studies and a structural model of $\gamma\text{-Al}_2\text{O}_3$ in the literature, we concluded that the anchoring sites of the isolated Ag(I) species on $\gamma\text{-Al}_2\text{O}_3$ are the $\text{HO-}\mu_1\text{-Al}_{\text{VI}}$ sites on the (100) surface adjacent to the strong Lewis acid (Al_{IV}) sites on the (110) surface.⁴² Based on the consistent DFT and experimental IR data, it is concluded that the $\text{HO-}\mu_1\text{-Al}_{\text{VI}}$ site on the (100)–(110) step edge is the anchoring site of Ag. After sintering, the isolated $\text{AgO-}\mu_1\text{-Al}_{\text{VI}}$ species aggregate to form Ag metal NPs to regenerate the $\text{HO-}\mu_1\text{-Al}_{\text{VI}}$ sites. In the subsequent oxidative treatment, the Ag metal NPs undergo redispersion to regenerate the original $\text{AgO-}\mu_1\text{-Al}_{\text{VI}}$ species.⁴² *In situ* DRIFT analysis of the four Ag/ Al_2O_3 samples after sintering treatment was used for *in situ* monitoring of the changes in the $\text{HO-}\mu_1\text{-Al}_{\text{VI}}$ sites during the oxidative redispersion process. First, the sample was reduced



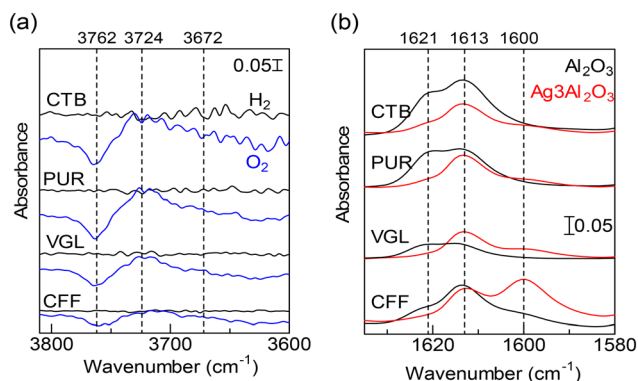


Fig. 3 (a) *In situ* DRIFT spectra of OH stretching on four types of Ag(3 wt%)-loaded Al_2O_3 after H_2 (black) and O_2 (blue) treatment at 500 °C. The spectra after O_2 treatment were based on the background spectra taken after the H_2 reduction. (b) *In situ* IR spectra of pyridine adsorbed at 200 °C on four types of $\gamma\text{-Al}_2\text{O}_3$ (black) and $\text{Ag}_3/\text{Al}_2\text{O}_3$ (red) pre-oxidized at 500 °C in 10% O_2/He for 0.5 h.

in 2% H_2 at 500 °C (0.5 h) followed by He purging, and IR spectra of the reduced samples (black lines in Fig. 3a) were obtained. The sample was then oxidized by 10% O_2 at 500 °C (0.5 h), and the IR spectra (blue lines in Fig. 3a) were obtained. For the four samples, a negative band centered around 3762 cm^{-1} appeared after re-oxidation by O_2 ; the intensity of this negative band increased in the order $\text{CTB} > \text{PUR} > \text{VGL} > \text{CFF}$. This order is consistent with the order of the catalytic activity (Table 1) and sintering resistance of supported Ag on alumina (Fig. 1).

In separate IR (transmission) experiments, pyridine adsorption on pre-oxidized IR disks of Al_2O_3 and $\text{Ag}/\text{Al}_2\text{O}_3$ was studied at 200 °C. For all samples, the band intensities of pyridine on the strong Lewis acid (Al_{IV}) sites (1621 cm^{-1}) of $\text{Ag}/\text{Al}_2\text{O}_3$ (red lines in Fig. 3b) were markedly lower than those of Al_2O_3 (black lines in Fig. 3b). This suggests that the Ag species in the form of $\text{AgO}-\mu_1\text{-Al}_{\text{VI}}$ decreased the Lewis acidity of the adjacent $\text{Al}_{\text{IV}}^{3+}$ sites because of the electronic effect of the Ag species. Fig. 4a presents a plot of the intensity

of the strong Lewis acid (Al_{IV}) sites (1621 cm^{-1}) of the Ag-free Al_2O_3 samples in Fig. 3b versus the intensity of the negative band of $\text{HO}-\mu_1\text{-Al}_{\text{VI}}$ (3762 cm^{-1}) observed due to re-oxidation of the sintered $\text{Ag}/\text{Al}_2\text{O}_3$ samples (Fig. 3a). A linear relationship was observed, providing additional evidence to support our previously reported conclusion⁴² that the anchoring sites of Ag on $\gamma\text{-Al}_2\text{O}_3$ are the $\text{HO}-\mu_1\text{-Al}_{\text{VI}}$ sites on the (100) surface adjacent to the strong Lewis acid (Al_{IV}) sites on the (110) surface at the (100)–(110) step edge. Fig. 4b presents a plot of the average sizes of the Ag NPs on the $\text{Ag}/\text{Al}_2\text{O}_3$ samples after sintering at 800 °C (Fig. 1) versus the intensity of the negative band of $\text{HO}-\mu_1\text{-Al}_{\text{VI}}$ (Fig. 3a). The size of the Ag metal NPs decreased with an increase in the number of $\text{HO}-\mu_1\text{-Al}_{\text{VI}}$ sites on the alumina surfaces, which demonstrates that the anchored Ag species in the form of $\text{AgO}-\mu_1\text{-Al}_{\text{VI}}$ play a significant role in the sintering resistance under reductive conditions at high temperatures.

In situ observation of oxidative dispersion

In situ time-resolved Ag *K*-edge XANES spectroscopy was used to characterize the structure of the Ag species during oxidative redispersion. Two Ag catalysts loaded on alumina with a relatively large amount (CTB) and a low number of $\text{HO}-\mu_1\text{-Al}_{\text{VI}}$ sites (VGL), Ag_3/CTB and Ag_3/VGL , pre-reduced by H_2 (800 °C), were exposed to $\text{NO} + \text{O}_2$ at 500 °C, while monitoring the XANES spectra as a function of time (Fig. 5). The EXAFS features (Fig. 5(a and b) and Table 2) of the sintered Ag_3/CTB (9.3 Ag–Ag bonds at 2.78 Å) and Ag_3/VGL (7.4 Ag–Ag bonds at 2.82 Å) show the absence of Ag^+ species on alumina and the presence of Ag metal NPs as major species. According to the method described in our previous study,⁴² LCF analysis of the spectra was performed in the energy range of 25 500–25 650 eV using the spectra of the two reference samples: Ag^+ ion-exchanged CHA zeolite for the isolated $\text{Ag}(\text{i})$ species and $\text{Ag}(10 \text{ wt\%})$ -loaded low surface area α -, θ - Al_2O_3 for the Ag metal NPs. LCF analysis of the samples at $t = 0 \text{ s}$ shows that Ag metal NPs are the dominant Ag

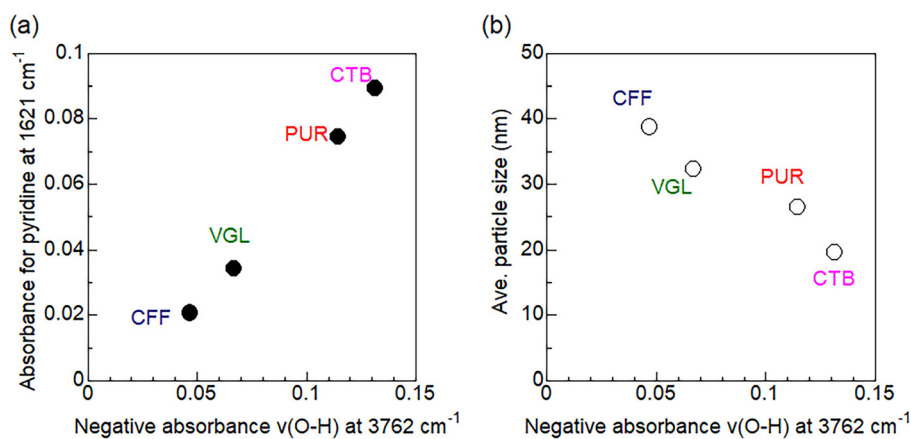


Fig. 4 (a) IR intensity of adsorbed pyridine (Fig. 3b) and (b) average particle size of Ag NPs (Fig. 1) versus IR intensity of negative peak due to $\text{HO}-\mu_1\text{-Al}_{\text{VI}}$ sites (Fig. 3a) on $\text{Ag}(3 \text{ wt\%})$ -loaded Al_2O_3 .



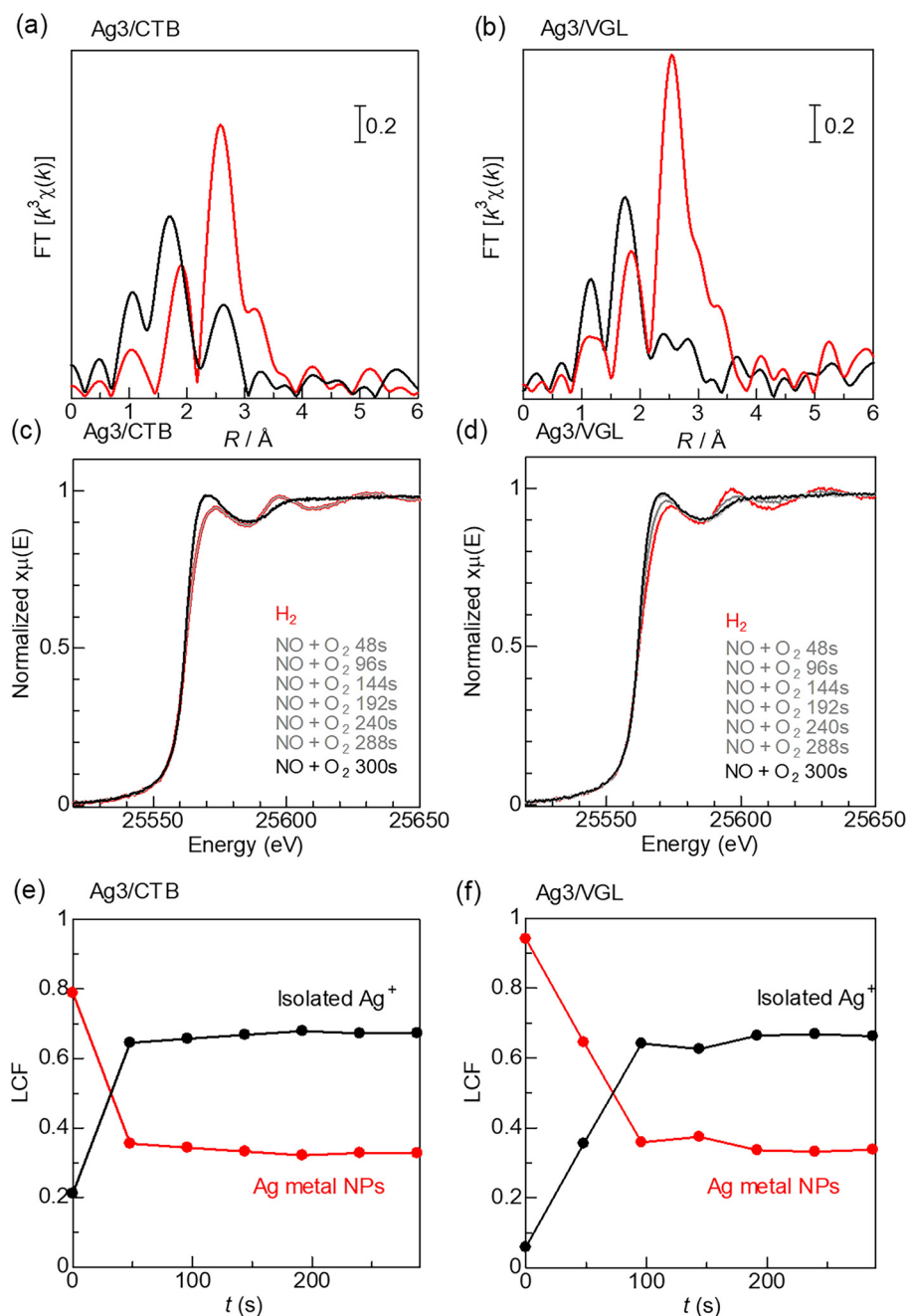


Fig. 5 *In situ* Ag K-edge EXAFS (a and b) and XANES (c and d) profiles of (a and c) Ag3/CTB and (b and d) Ag3/VGL during re-oxidation by $\text{NO} + \text{O}_2$ for 300 s (black spectra) at 500 °C after H_2 treatment at 800 °C (red spectra). Time-dependence LCF fraction of Ag metal NPs and isolated Ag^+ in (e) Ag3/CTB and (f) Ag3/VGL. Flow rate = 1000 mL min^{-1} ; sample weight = 136.8 mg.

species in the sintered catalysts. With an increase in the time of oxidation by $\text{NO} + \text{O}_2$, the fraction of $\text{Ag}(\text{i})$ species increased and that of Ag metal NPs decreased. This indicates that the Ag metal NPs undergo oxidative dispersion to form isolated $\text{Ag}(\text{i})$ species. Some of the Ag metal NPs on Ag3/CTB were converted to isolated $\text{Ag}(\text{i})$ species within 48 s, whereas the oxidative dispersion was completed in 96 s for Ag3/VGL. This indicates that oxidative redispersion of the Ag metal NPs is faster for alumina with a larger number of surface $\text{HO}-\mu_1$ -

Al_{VI} sites (CTB). Oxidation by $\text{NO} + \text{O}_2$ treatment for 300 s decreased the intensity of the Ag–Ag contribution to the EXAFS peak, accompanied by the appearance of peaks corresponding to Ag–O coordination (Fig. 5(a) and (b) and Table 2). The EXAFS results indicate that some of the Ag metal NPs were converted to isolated $\text{Ag}(\text{i})$ species bonded to alumina, which is consistent with the XANES results.

Similar experiments for the redispersion process were performed using *in situ* diffuse reflectance UV-vis



Table 2 Ag *K*-edge EXAFS curve-fitting analysis of Ag₃/Al₂O₃

Sample	Shell	CN ^a	<i>R</i> ^b /Å	$\sigma^{2c}/\text{\AA}^2$	<i>R</i> _f ^d /%
Sintered Ag ₃ /CTB	Ag–Ag	8.9	2.89	0.0237	2.9
Re-oxidized Ag ₃ /CTB	Ag–O	1.1	2.25	0.0682	2.1
	Ag–Ag	1.6	2.71	0.0208	2.4
Sintered Ag ₃ /VGL	Ag–Ag	8.3	2.76	0.0247	2.9
Re-oxidized Ag ₃ /VGL	Ag–O	1.1	2.22	0.0060	2.1
	Ag–Ag	4.6	2.74	0.0382	2.4

^a Coordination number. ^b Bond distance. ^c Debye–Waller factor.^d Residual factor.

spectroscopy.^{19,44} The UV-vis spectra of the four different Ag/Al₂O₃ samples pre-reduced at 800 °C showed a broad band around 400–800 nm, assignable to the small Ag metal NPs (black lines in Fig. 6). The intensity of the band at 750 nm was monitored as a function of time under NO + O₂ at 400 °C (Fig. 7a). Oxidation by NO + O₂ for 0.5 h decreased the intensity of the band at 400–800 nm due to the Ag metal NPs (blue lines in Fig. 6). Fig. 8a presents a plot of the decrease in the intensity of the UV-vis band at 750 nm (relative amount of redispersed Ag NPs) *versus* the intensity of the negative peak in the IR profile arising from the HO-μ₁-Al_{VI} sites. Conversion of the Ag metal NPs to Ag(I) species

increased with increasing number of HO-μ₁-Al_{VI} sites on alumina, indicating that the HO-μ₁-Al_{VI} sites act as anchoring sites for the dispersed Ag(I) species.

The kinetic curves in Fig. 7a were numerically differentiated to obtain the plots of the initial slope of the kinetic curve ($\Delta\text{KM}/\Delta t$) *versus* time (Fig. 7b). The maximum values of $\Delta\text{KM}/\Delta t$ in the initial period correspond to the initial rates for redispersion of the Ag metal NPs into Ag(I) species. The rates depend on the type of alumina support and changed in the order CTB > PUR > VGL > CFF. This order is consistent with the order of the catalytic activity (Table 1) and sintering resistance of Ag supported on alumina (Fig. 1). Fig. 8a presents the plot of the initial rates for the redispersion of Ag metal NPs (Fig. 7b) as a function of the intensity of the negative band of HO-μ₁-Al_{VI}. The rate of redispersion of the Ag metal NPs increased with an increase in the number of HO-μ₁-Al_{VI} sites, which shows that alumina with a larger number of HO-μ₁-Al_{VI} sites leads to more rapid redispersion under oxidative conditions.

In the H₂-NH₃-SCR and H₂-C₃H₆-SCR employing the Ag/Al₂O₃ catalysts, reductive aggregation (Ag⁺ → Ag metal) by H₂ and oxidative dispersion (Ag metal → Ag⁺) by NO + O₂ may compete with each other; hence, the relative amount of Ag metal and Ag(I) species depends on the number of HO-μ₁-Al_{VI}

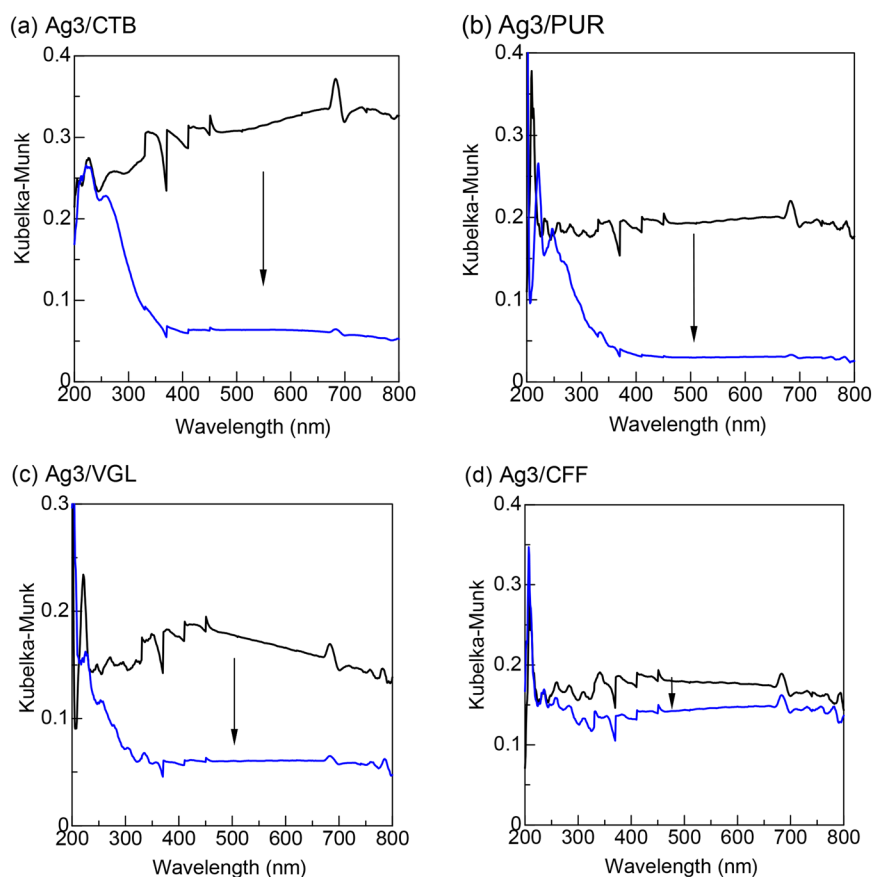


Fig. 6 (a) *In situ* UV spectra of (a) Ag₃/CTB, (b) Ag₃/PUR, (c) Ag₃/VGL, and (d) Ag₃/CFF after sintering treatment (black), followed by NO + O₂ treatment at 400 °C for 0.5 h (blue).



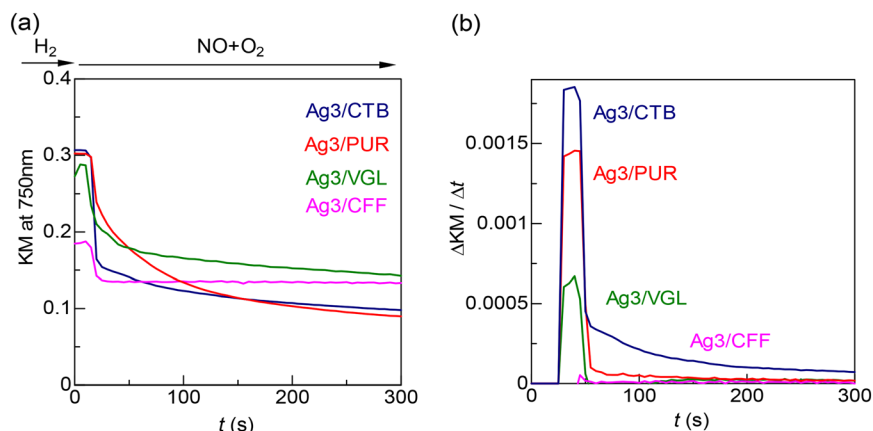


Fig. 7 (a) Time-dependence of relative amount of Ag NPs (UV-vis intensity (KM) at 750 nm) on Ag₃/Al₂O₃ samples under NO + O₂ at 400 °C and (b) redispersion rate of Ag NPs, estimated by numerical differentiation ($\Delta\text{KM}/\Delta t$) of the kinetic curves vs. time.

sites on the different alumina types. To quantitatively discuss the effect of the number of anchoring sites on the SCR activity of the Ag/Al₂O₃ catalysts, the NO conversion (Table 1) in the H₂-NH₃-SCR at 150 °C and H₂-C₃H₆-SCR at 400 °C was plotted *versus* the IR intensity of the negative peak due to the HO-μ₁-Al_VI sites (Fig. 9). For both reactions, the NO conversion increased with increasing number of HO-μ₁-Al_VI sites, which clearly indicates that Al₂O₃ with a larger number of surface HO-μ₁-Al_VI sites is preferable as a support material for the H₂-assisted SCR promoted by Ag/Al₂O₃ catalysts. A larger number of anchoring sites should lead to a higher fraction of highly dispersed Ag(i) species as active species for the SCR, rather than Ag metal NPs, resulting in higher NO conversion.

Redispersion mechanism

To discuss the role of NO and O₂ during redispersion of the Ag metal NPs, we carried out *in situ* diffuse reflectance UV-vis experiments of Ag₃/CTB pre-reduced by H₂ at 800 °C. The

intensity of the UV-vis band at 750 nm, assignable to Ag metal NPs, was monitored as a function of oxidation time under NO, O₂, or NO + O₂ atmosphere at 500 °C (Fig. 10). As the sample was exposed to O₂, or NO + O₂ atmosphere at 500 °C, the peak intensity for Ag NPs decreased with time, while the intensity did not decrease under NO. The redispersion rate of Ag NPs, estimated from the slope of the kinetic curves, changes in the order NO + O₂ > O₂ ≫ NO. The result indicates that the redispersion of Ag metal NPs occurs in O₂ and NO + O₂ at 500 °C, and the redispersion in O₂ is promoted by NO.

As proposed in our previous work,⁴² the redispersion mechanism under NO + O₂ is described by the following reactions, where AgNO₃ species acts as mobile Ag species.

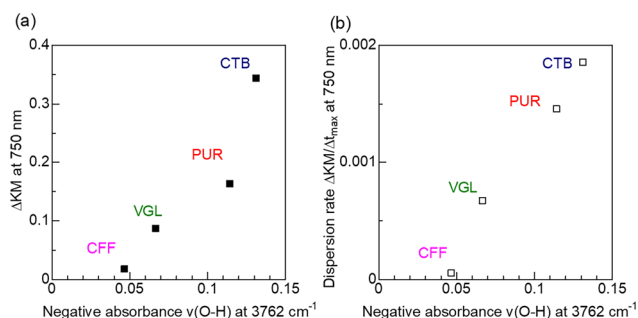


Fig. 8 (a) The relative amount of redispersed Ag NPs (ΔKM value in Fig. 6) and (b) the initial rates of Ag NPs re-dispersion (the maximum $\Delta\text{KM}/\Delta t$ value in Fig. 7b), *versus* IR intensity of negative peak due to HO-μ₁-Al_VI sites (Fig. 3a) for Ag₃/Al₂O₃ samples.

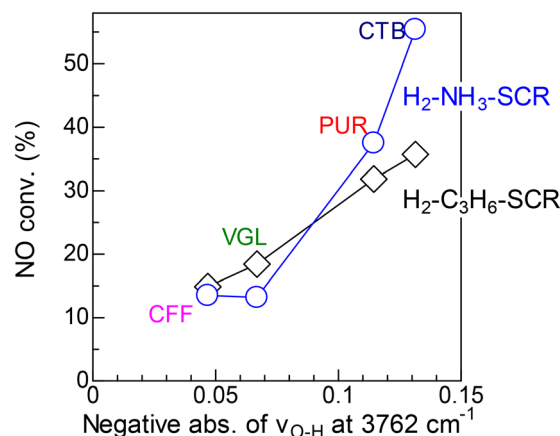


Fig. 9 NO conversion (from Table 1) for H₂-NH₃-SCR at 150 °C and H₂-C₃H₆-SCR at 400 °C *versus* IR intensity of negative peak due to HO-μ₁-Al_VI sites (Fig. 3a) for Ag₃/Al₂O₃ samples. Flow rate = 100 mL min⁻¹; sample weight = 15 mg.



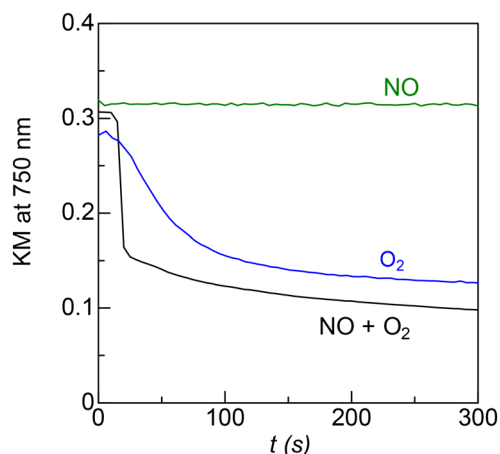


Fig. 10 Time dependence of the UV-vis signal intensity due to Ag NPs during reoxidation by (black) 500 ppm NO, (blue) 10% O₂, and (green) 500 ppm NO + 10% O₂ at 500 °C. The Ag3/CTB sample was pre-reduced in 2% H₂ at 800 °C.

The redispersion mechanism under O₂ is described by the following reaction.



Under O₂ at 500 °C, metallic Ag⁰ species at the interface between Ag metal NPs and alumina may be oxidized by O₂ to yield Ag⁺ ions exchanged by Al-OH groups (Al-OAg). The surface Ag⁺ is exchangeable to H⁺ of adjacent Al-OH groups and moves across the alumina surface owing to the concentration gradient of the Ag⁺ cations. The higher dispersion rate under NO + O₂ than under O₂ can be due to the higher Ag⁰ oxidation rates or higher migration rates of mobile Ag(I) species under NO + O₂.

Redispersion of Ag NPs during H₂-C₃H₆-SCR reaction

The oxidative conversion of inactive Ag NPs into Ag⁺ species as catalytically active species may result in *in situ* regeneration of the sintered catalysts during SCR reaction, shown in Fig. 11. To verify this hypothesis, we carried out the H₂-C₃H₆-SCR reaction by the Ag1/CTB catalyst pre-reduced by H₂ at 800 °C. The STEM image of the sintered catalyst shows large Ag NPs. The initial NO conversion of the sintered catalyst (6%) was lower than that of the fresh Ag1/CTB (17%). The NO_x conversion of the sintered Ag1/CTB gradually increased with time of the H₂-C₃H₆-SCR reaction and reached the value of the fresh Ag1/CTB (dashed red line). The result demonstrates that the oxidative redispersion of aggregated Ag NPs and resulting regeneration of the catalytic activity are possible under catalytic conditions.

4. Conclusions

Ag/Al₂O₃ catalysts were prepared using four types of commercial alumina sources. The effect of the relative amount of on-top OH groups on octahedral Al (HO-μ₁-Al_{VI})

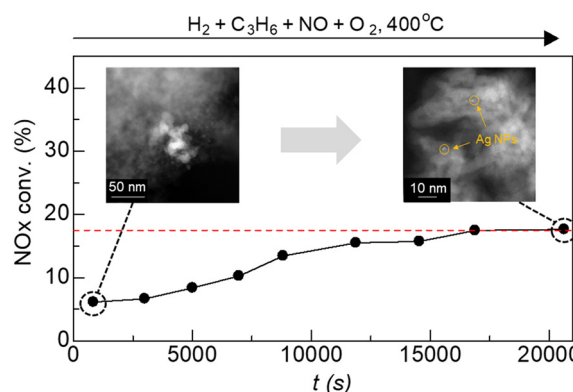


Fig. 11 Time course of NO_x conversion for H₂-C₃H₆-SCR by the sintered Ag1/CTB catalyst (pre-reduced by H₂ at 800 °C); the dashed red line corresponds to the NO_x conversion of the fresh Ag1/CTB catalyst. Insets: STEM images of the sintered Ag1/CTB before and after the H₂-C₃H₆-SCR reaction.

on (1) the amount of unsaturated Al_{IV}³⁺ sites, (2) the sintering resistance of Ag/Al₂O₃, (3) the rate of Ag redispersion, and (4) the catalytic activity of Ag/Al₂O₃ was investigated. The number of strong Lewis acid (unsaturated Al_{IV}³⁺) sites on the Ag-free γ-Al₂O₃ supports increased with an increase in the number of HO-μ₁-Al_{VI} sites. Combined with the results in our previous report,⁴² the data demonstrate that the HO-μ₁-Al_{VI} site on the (100) surface adjacent to the unsaturated Al_{IV}³⁺ site on the (110) surface at the (100)-(110) step edge is a general model for the anchoring sites of Ag on γ-Al₂O₃. The anchored Ag species, AgO-μ₁-Al_{VI}, underwent sintering to yield Ag metal NPs after H₂ reduction at 800 °C. The mean size of the Ag metal NPs after sintering decreased with an increase in the number of anchoring sites on the alumina surface. Under NO + O₂, the sintered Ag/Al₂O₃ catalysts undergo oxidative redispersion to regenerate the AgO-μ₁-Al_{VI} sites. The amount of redispersed Ag metal and the initial rate of the redispersion process increase with the number of HO-μ₁-Al_{VI} sites, which demonstrates that the anchored Ag species are in the form of AgO-μ₁-Al_{VI}. These results show that the HO-μ₁-Al_{VI} site adjacent to the unsaturated Al_{IV}³⁺ site on γ-Al₂O₃ (anchoring site of Ag) plays an important role in the sintering resistance and redispersion of the supported Ag species. The activity of these catalysts for H₂-assisted SCR of NO by NH₃ or C₃H₆ increased with an increase in the number of HO-μ₁-Al_{VI} sites. In summary, the present results provide a simple concept for designing sintering-resistant Ag/Al₂O₃ catalysts for SCR; γ-Al₂O₃ with a larger amount of surface HO-μ₁-Al_{VI} sites is a preferable support for H₂-assisted SCR by Ag/Al₂O₃ catalysts because the support with a larger number of anchoring sites provides a larger number of AgO-μ₁-Al_{VI} sites as active sites for H₂-assisted SCR, possibly *via* dynamic sintering/redispersion cycles.

Conflicts of interest

There are no conflicts to declare.



Acknowledgements

This research was supported by the JST-CREST project JPMJCR17J3, KAKENHI (Grant No. 20H02518, 20H02775, 20KK0111, 21H04626 and 22K14538), the Joint Usage/Research Center for Catalysis, and the MEXT project IRCCS. H. K. acknowledges the JSPS Research Fellowship for Young Scientists (Grant No. 21J11913). XAS measurements were performed at the SPring-8 BL-14B2 beamline at JASRI (proposal No. 2021A1615).

References

- 1 K. Shimizu, J. Shibata, H. Yoshida, A. Satsuma and T. Hattori, Silver-Alumina Catalysts for Selective Reduction of NO by Higher Hydrocarbons: Structure of Active Sites and Reaction Mechanism, *Appl. Catal., B*, 2001, **30**, 151–162.
- 2 H. Deng, Y. Yu, F. Liu, J. Ma, Y. Zhang and H. He, Nature of Ag Species on Ag/ γ -Al₂O₃: A Combined Experimental and Theoretical Study, *ACS Catal.*, 2014, **4**, 2776–2784.
- 3 H. Deng, Y. Yu and H. He, Discerning the Role of Ag-O-Al Entities on Ag/ γ -Al₂O₃ Surface in NO_x Selective Reduction by Ethanol, *J. Phys. Chem. C*, 2015, **119**, 3132–3142.
- 4 J. P. Breen, R. Burch, C. Hardacre, C. J. Hill, B. Krutzsch, B. Bandl-Konrad, E. Jobson, L. Cider, P. G. Blakeman, L. J. Peace, M. V. Twigg, M. Preis and M. Gottschling, An Investigation of the Thermal Stability and Sulphur Tolerance of Ag/ γ -Al₂O₃ Catalysts for the SCR of NO_x with Hydrocarbons and Hydrogen, *Appl. Catal., B*, 2007, **70**, 36–44.
- 5 K. Hayashizaki, T. Jibiki, K. Inoue, Y. Koyanagi, S. Tanaka, H. Tongu, H. Hirabayashi and S. Sato, After-Treatment System of Medium Duty Engines Using Diesel Fuel as a Reducing Agent for NO_x Reduction, *SAE [Tech. Pap.]*, 2018, **1**, 0345.
- 6 J. Shibata, K. Shimizu, S. Satokawa, A. Satsuma and T. Hattori, Promotion Effect of Hydrogen on Surface Steps in SCR of NO by Propane over Alumina-Based Silver Catalyst as Examined by Transient FT-IR, *Phys. Chem. Chem. Phys.*, 2003, **5**, 2154–2160.
- 7 K. Shimizu, M. Katagiri, S. Satokawa and A. Satsuma, Applied Catalysis B : Environmental Sintering-Resistant and Self-Regenerative Properties of Ag/SnO₂ Catalyst for Soot Oxidation, *Appl. Catal., B*, 2011, **108–109**, 39–46.
- 8 H. Kannisto, M. Skoglundh, K. Arve, E. Olsson and H. Härelind, Direct Observation of Atomically-Resolved Silver Species on a Silver Alumina Catalyst Active for Selective Catalytic Reduction of Nitrogen Oxides, *Catal. Sci. Technol.*, 2019, **9**, 6213–6216.
- 9 S. Tamm, N. Vallim, M. Skoglundh and L. Olsson, The Influence of Hydrogen on the Stability of Nitrates during H₂-Assisted SCR over Ag/Al₂O₃ Catalysts - A DRIFT Study, *J. Catal.*, 2013, **307**, 153–161.
- 10 S. T. Korhonen, A. M. Beale, M. A. Newton and B. M. Weckhuysen, New Insights into the Active Surface Species of Silver Alumina Catalysts in the Selective Catalytic Reduction of NO, *J. Phys. Chem. C*, 2011, **115**, 885–896.
- 11 N. Bogdanchikova, F. C. Meunier, M. Avalos-Borja, J. P. Breen and A. Pestryakov, On the Nature of the Silver Phases of Ag/Al₂O₃ Catalysts for Reactions Involving Nitric Oxide, *Appl. Catal., B*, 2002, **36**, 287–297.
- 12 P. Soon, M. Kyu, B. K. Cho, I. Nam and S. H. Oh, Effect of H₂ on DeNO_x Performance of HC-SCR over Ag/Al₂O₃: Morphological, Chemical, and Kinetic Changes, *J. Catal.*, 2013, **301**, 65–76.
- 13 F. Wang, J. Ma, S. Xin, Q. Wang, J. Xu, C. Zhang, H. He and X. Cheng Zeng, Resolving the Puzzle of Single-Atom Silver Dispersion on Nanosized γ -Al₂O₃ Surface for High Catalytic Performance, *Nat. Commun.*, 2020, **11**, 1–11.
- 14 M. Richter, R. Fricke and R. Eckelt, Unusual Activity Enhancement of NO Conversion over Ag/Al₂O₃ by Using a Mixed NH₃/H₂ Reductant under Lean Conditions, *Catal. Lett.*, 2004, **94**, 115–118.
- 15 E. V. Kondratenko, V. A. Kondratenko, M. Richter and R. Fricke, Influence of O₂ and H₂ on NO Reduction by NH₃ over Ag/Al₂O₃: A Transient Isotopic Approach, *J. Catal.*, 2006, **239**, 23–33.
- 16 V. A. Kondratenko, U. Bentrup, M. Richter, T. W. Hansen and E. V. Kondratenko, Mechanistic Aspects of N₂O and N₂ Formation in NO Reduction by NH₃ over Ag/Al₂O₃: The Effect of O₂ and H₂, *Appl. Catal., B*, 2008, **84**, 497–504.
- 17 G. Xu, H. Wang, Y. Yu and H. He, Role of Silver Species in H₂-NH₃-SCR of NO_x over Ag/Al₂O₃ Catalysts: Operando Spectroscopy and DFT Calculations, *J. Catal.*, 2021, **395**, 1–9.
- 18 K. Shimizu and A. Satsuma, Hydrogen Assisted Urea-SCR and NH₃-SCR with Silver-Alumina as Highly Active and SO₂-Tolerant de-NO_x Catalysis, *Appl. Catal., B*, 2007, **77**, 202–205.
- 19 K. Shimizu and A. Satsuma, Reaction Mechanism of H₂-Promoted Selective Catalytic Reduction of NO with NH₃ over Ag/Al₂O₃, *J. Phys. Chem. C*, 2007, **111**, 2259–2264.
- 20 G. Xu, J. Ma, L. Wang, Z. Lv, S. Wang and Y. Yu, Mechanism of the H₂ Effect on NH₃-Selective Catalytic Reduction over Ag/Al₂O₃: Kinetic and Diffuse Reflectance Infrared Fourier Transform Spectroscopy Studies, *ACS Catal.*, 2019, **9**, 10489–10498.
- 21 Q. Wan, S. Hu, J. Dai, C. Chen and W. X. Li, First-Principles Kinetic Study for Ostwald Ripening of Late Transition Metals on TiO₂ (110), *J. Phys. Chem. C*, 2019, **123**, 1160–1169.
- 22 C. K. Narula and G. M. Stocks, Ab Initio Density Functional Calculations of Adsorption of Transition Metal Atoms on θ -Al₂O₃(010) Surface, *J. Phys. Chem. C*, 2012, **116**, 5628–5636.
- 23 E. M. Dietze and P. N. Plessow, Predicting the Strength of Metal – Support Interaction with Computational Descriptors for Adhesion Energies, *J. Phys. Chem. C*, 2019, **123**, 20443–20450.
- 24 G. Agostini, S. Usseglio, E. Groppo, M. J. Uddin, C. Prestipino, S. Bordiga, A. Zecchina, P. L. Solari and C. Lamberti, From Isolated Ag⁺ Ions to Aggregated Ag⁰ Nanoclusters in Silver-Exchanged Engelhard Titanosilicate (ETS-10) Molecular Sieve: Reversible Behavior, *Chem. Mater.*, 2009, **21**, 1343–1353.
- 25 K. Shimizu, K. Sawabe and A. Satsuma, Self-Regenerative Silver Nanocluster Catalyst for CO Oxidation, *ChemCatChem*, 2011, **3**, 1290–1293.
- 26 G. Busca, Structural, Surface, and Catalytic Properties of Aluminas, *Adv. Catal.*, 2014, **57**, 319–404.



- 27 F. Rascón, R. Wischert and C. Copéret, Molecular Nature of Support Effects in Single-Site Heterogeneous Catalysts: Silica vs. Alumina, *Chem. Sci.*, 2011, **2**, 1449–1456.
- 28 E. J. Jang, J. Lee and J. H. Kwak, Morphology Change and Phase Transformation of Alumina Related to Defect Sites and Its Use in Catalyst Preparation, *Catal. Today*, 2020, **352**, 323–328.
- 29 J. H. Kwak, J. Z. Hu, D. H. Kim, J. Szanyi and C. H. F. Peden, penta-Coordinated Al^{3+} Ions as Preferential Nucleation Sites for BaO on $\gamma\text{-Al}_2\text{O}_3$: An Ultra-High-Magnetic Field ^{27}Al MAS NMR Study, *J. Catal.*, 2007, **251**, 189–194.
- 30 J. H. Kwak, J. Hu, A. Lukaski, D. H. Kim, J. Szanyi and C. H. F. Peden, Role of pentacoordinated Al^{3+} Ions in the High Temperature Phase Transformation of $\gamma\text{-Al}_2\text{O}_3$, *J. Phys. Chem. C*, 2008, **112**, 9486–9492.
- 31 T. K. Phung, A. Lagazzo, M. Á. Rivero Crespo, V. Sánchez Escribano and G. Busca, A Study of Commercial Transition Aluminas and of Their Catalytic Activity in the Dehydration of Ethanol, *J. Catal.*, 2014, **311**, 102–113.
- 32 K. Murata, T. Shiotani, J. Ohyama, R. Wakabayashi, H. Maruoka, T. Kimura and A. Satsuma, Relationship between penta-Coordinated Al^{3+} Sites in the Al_2O_3 Supports and CH_4 Combustion Activity of $\text{Pd}/\text{Al}_2\text{O}_3$ Catalysts, *Catal. Sci. Technol.*, 2021, **11**, 2374–2378.
- 33 X. Liu, DRIFTS Study of Surface of γ -Alumina and Its Dehydroxylation, *J. Phys. Chem. C*, 2008, **112**, 5066–5073.
- 34 S. Srinivasan, C. R. Narayanan and A. K. Datye, The Role of Sodium and Structure on the Catalytic Behavior of Alumina: II. IR Spectroscopy, *Appl. Catal., A*, 1995, **132**, 289–308.
- 35 D. T. Lundie, A. R. McInroy, R. Marshall, J. M. Winfield, P. Jones, C. C. Dudman, S. F. Parker, C. Mitchell and D. Lennon, Improved Description of the Surface Acidity of η -Alumina, *J. Phys. Chem. B*, 2005, **109**, 11592–11601.
- 36 T. K. Phung, C. Herrera, M. Á. Larrubia, M. García-Diéguez, E. Finocchio, L. J. Alemany and G. Busca, Surface and Catalytic Properties of Some $\gamma\text{-Al}_2\text{O}_3$ Powders, *Appl. Catal., A*, 2014, **483**, 41–51.
- 37 X. Liu and R. E. Truitt, DRFT-IR Studies of the Surface of γ -Alumina, *J. Am. Chem. Soc.*, 1997, **119**, 9856–9860.
- 38 C. Morterra and G. Magnacca, A Case Study: Surface Chemistry and Surface Structure of Catalytic Aluminas, as Studied by Vibrational Spectroscopy of Adsorbed Species, *Catal. Today*, 1996, **27**, 497–532.
- 39 M. Digne, P. Sautet, P. Raybaud, P. Euzen and H. Toulhoat, Use of DFT to Achieve a Rational Understanding of Acid-Base Properties of γ -Alumina Surfaces, *J. Catal.*, 2004, **226**, 54–68.
- 40 J. Lee, E. J. Jang, H. Y. Jeong and J. H. Kwak, Critical Role of (100) Facets on $\gamma\text{-Al}_2\text{O}_3$ for Ethanol Dehydration: Combined Efforts of Morphology-Controlled Synthesis and TEM Study, *Appl. Catal., A*, 2018, **556**, 121–128.
- 41 A. Dyan, P. Cenedese and P. Dubot, Physical Properties of γ Alumina Surface Hydroxyls Revisited through a Large Scale Periodic Quantum-Chemistry Approach, *J. Phys. Chem. B*, 2006, **110**, 10041–10050.
- 42 H. Kubota, S. Mine, T. Toyao, Z. Maeno and K. I. Shimizu, Redox-Driven Reversible Structural Evolution of Isolated Silver Atoms Anchored to Specific Sites on $\gamma\text{-Al}_2\text{O}_3$, *ACS Catal.*, 2022, **12**, 544–559.
- 43 B. Ravel and M. Newville, ATHENA, ARTEMIS, HEPHAESTUS: Data Analysis for X-Ray Absorption Spectroscopy Using IFEFFIT, *J. Synchrotron Radiat.*, 2005, **12**, 537–541.
- 44 B. Inceesungvorn, J. López-Castro, J. J. Calvino, S. Bernal, F. C. Meunier, C. Hardacre, K. Griffin and J. J. Delgado, Nano-Structural Investigation of $\text{Ag}/\text{Al}_2\text{O}_3$ Catalyst for Selective Removal of O_2 with Excess H_2 in the Presence of C_2H_4 , *Appl. Catal., A*, 2011, **391**, 187–193.

